Study on anisotropy of cosmic ray distribution with a small array of water Cherenkov detectors

F. Sheidaei,[1] M. Bahmanabadi,[1,2,*] A. Keivani,[1] M. Khakian Ghomi,[2] J. Samimi,[1,2] and A. Shadkam[1]

[1]*Department of Physics, Sharif University of Technology, P.O. Box 11365-9161, Tehran, Iran*

[2]*ALBORZ Observatory, Sharif University of Technology, Tehran, Iran*

(Received 8 May 2007; revised manuscript received 4 July 2007; published 26 October 2007)

The study of the anisotropy of the arrival directions is an essential tool to investigate the origin and propagation of cosmic ray primaries. A simple way of recording many cosmic rays is to record coincidences between a number of detectors. We have monitored multi-TeV cosmic rays by a small array of water Cherenkov detectors in Tehran (35°43′ N, 51°20′ E, 1200 m above sea level). More than 1.1×10^6 extensive air shower events were recorded. In addition to the Compton-Getting effect due to the motion of the Earth in the Galaxy, an anisotropy has been observed which is due to a unidirectional anisotropy of cosmic ray flow along the Galactic arms.

DOI: 10.1103/PhysRevD.76.082002 PACS numbers: 96.50.sd, 13.85.Tp

I. INTRODUCTION

Although cosmic rays (CRs) have been known for almost a century, their origin remains uncertain, mostly because their trajectories are bent by Galactic magnetic fields and they do not individually point back to their sources. Cosmic rays in the lower energy range have gyro radii of about 1 pc or less in typical galactic magnetic fields (a proton with an energy of 10^{15} eV would have a gyro radius of 1 pc in a 1 μG field). Moreover, since these fields are chaotic on scales ranging at least from 10^8 cm to 10^{20} cm [1], the transport of CRs is diffusive up to high energies, which tends to make their angular distribution isotropic. Therefore, even collectively, the CR arrival directions hold virtually no information about the source distribution in space. However, as the energy of the CRs increases, it can appear either because the diffusive approximation does not hold anymore, or because the diffusion coefficient becomes large enough to reveal intrinsic inhomogeneities in the source distribution. Specifically, even if the diffusive regime holds, the density of CR sources in the Galaxy is believed to be larger in the inner regions than in the outer ones, and this can cause a slightly higher CR flux coming from the Galactic center than from the anticenter. Meanwhile, the global CR streaming away from the Galactic plane (towards the halo) can be a source of measurable anisotropy. However, the detailed angular distribution of CRs is quite hard to predict, even if we assume a definite source distribution, because it also depends on the propagation conditions, which are related to both large scale and small scale magnetic field configurations, and on the position of the Earth relative to major magnetic structures, such as the local Galactic arm.

From a general point of view, the characterization of the CR anisotropy provides useful information to constrain the Galactic cosmic ray (GCR) diffusion models, notably the effective diffusion coefficients, related to the magnetic field structure. Indeed, the level of CR anisotropy depends on the diffusion coefficient D: in a simple model where CR sources are homogeneously distributed in a disk of thickness $2h$ and the CRs are confined in a halo of height H, the anisotropy at a distance z above the Galactic plane ($z < h$) is estimated as $\Delta \simeq 3D/cH \times z/h$ [2]. The deviation from isotropy is typically below 1% and can be as low as 0.03% [3]. Anisotropy measurements at various energies can thus provide crucial information about the energy dependence of the diffusion coefficient. This information is particularly important to constrain the GCR source spectrum, since it sets the relation between the source power law index and the observed one, through the energy dependent confinement of CRs in the Galaxy. This diffusion might be broad along the magnetic field lines which are in tubes of dimensions greater than the gyro radii. So the direction of the peak of the anisotropy would indicate the direction back towards the cosmic ray source, and the amplitude of the anisotropy would give information on the scattering process involved in the diffusion. Specifically, an estimate of the mean free path might be obtained.

The anisotropy is due to a combination of effects. In 1935 Compton and Getting [4] proposed that the motion of the solar system relative to the rest frame of the cosmic ray plasma should cause an energy independent dipole anisotropy with a maximum in the direction of motion. The Earth's rapid motion in space, resulting from the rotation of our Galaxy, causes variations in cosmic ray intensity fore and aft of the Earth's motion. Following Compton-Getting (1935), the magnitude of the anisotropy is expressed as

$$\eta = (\gamma + 2)\frac{u}{c}\cos\beta, \tag{1}$$

where γ denotes the power law index of the energy spectrum of cosmic rays, u is the velocity of the detector relative to the production frame of the cosmic rays (where they are presumed to be isotropic), c is the speed of light, and β is the cosmic ray direction relative to u; i.e. $\cos\beta$ is the projection of the cosmic ray along the forward

*bahmanabadi@sina.sharif.edu

direction of u. In fact, the value of $(\gamma + 2)\frac{u}{c}$ is $(f_{\max} - f_{\min})/(f_{\max} + f_{\min})$ with $f_{\max}$ the counting rate along the direction of the velocity and $f_{\min}$ along the contrary direction. The magnitude of the anisotropy is extremely small and independent of the cosmic ray energy. Our data will be analyzed in a sun-centered frame, and so if data accumulation is done over an integer number of solar years, it is only necessary that the orbital speed of the Earth around the sun (~ 30 km s^{-1}) be considered. The large effect due to the Galactic rotational speed (220 km s^{-1}) will cancel out as the data are averaged over this time [5]. Many experiments have been carried out for detection of this effect [5,6].

Doppler effect studies of globular clusters and extra galactic nebulae have revealed a motion of the Earth of about 220 km s^{-1} towards right ascension $\alpha \simeq 21$ h and declination $\delta \simeq 47°$N due chiefly to the rotation of the Galaxy. This motion, with a speed of about $0.1\%c$, will affect the intensity of the incoming cosmic rays by changing both the energy of the cosmic ray particles and the number received per second. Using the value of 220 km s^{-1} for u, and 2.7 for the spectral index, Eq. (1) gives a Compton Getting effect (CGE) amplitude of 0.345×10^{-2} for the fractional forward-backward asymmetry caused by the motion of the Earth in the Galaxy.

Other effects that can produce sidereal modulation are solar diurnal and seasonal changes in the atmospheric temperature and pressure. As the atmospheric temperature and pressure change during the course of a day, the balance of cosmic ray secondary particle interaction and decay changes. This propagates to changes in the detection rate that depend on the detector type (air shower, underground muon, surface muon) and on the energy threshold. These changes tend to have a strong Fourier component with a frequency of one solar day ($\simeq 365$ cycles/year) and one solar year (1 cycle/year). In some (but by no means all) experiments, the interplay between the daily and seasonal modulation can produce significant modulation in sideband frequencies of $\simeq (365 \pm 1)$ cycles/year [7]. The modulation with frequency 366 cycles/year appears as a sidereal modulation. The size of the atmospheric contribution to apparent sidereal anisotropy can be estimated from the amplitude of the pseudosidereal (365 cycles/year) frequency. If it is large, the atmospheric effect can be subtracted using the amplitude and phase of the pseudosidereal component. The anisotropy that remains after accounting for the Compton-Getting and atmospheric effects is due to solar and galactic effects. At the lowest energies (~ 100 GeV), the interplanetary magnetic field (IMF) produced by the solar wind effects the sidereal anisotropy: when the local IMF points toward the sun, the anisotropy peaks at about 18 hour right ascension, while it peaks at 6 hours when it points away [8,9]. The average over the two configurations produces a small, residual anisotropy peaking at around 2–4 hours. At higher energies, the local IMF plays a negligible role. Instead, the heliosphere extending to distances of order 100 AU is believed to induce anisotropy in cosmic rays with energies around 1 TeV [10,11]. Beyond this energy, the anisotropy is believed to be primarily of galactic origin. For instance, the galactic magnetic field around the solar system neighborhood could produce anisotropy. Also, an uneven distribution of sources of cosmic rays (presumably, mostly supernova remnants) may produce anisotropy. It is believed that star formation (and thus supernova remnants) occurs primarily in the spiral arms of the galaxy. The Earth is located at the inner edge of the Orion spur. Thus, in the direction of the Orion spur (galactic longitude between 60° and 270°) they are distributed nearby sources of cosmic rays, while in the complementary direction, they are much further away.

Because of small anisotropy, large data sets are required to make useful measurements which overcome the statistical uncertainties of counting experiments. A simple way of recording many cosmic rays is to record coincidences between a number of detectors. Few statistically significant anisotropies have been reported from extensive air shower experiments in the last two decades. Aglietta *et al.* (1996, EAS-TOP) [12] published an amplitude of $(3.7 \pm 0.6) \times 10^{-4}$ and phase $\phi = (1.8 \pm 0.5)$ hr local sidereal time (LST), at $E_\circ \approx 200$ TeV. Analyzing the Akeno experiment, Kifune *et al.* (1986) [13] reported results of about 2×10^{-3} at about 5 to 10 PeV. An overview of experimental results can be found in [14]. We have operated a small array of water Cherenkov detectors on the roof of the Physics Department at Sharif University of Technology in Tehran (35°43′ N, 51°20′ E, 1200 m a.s.l = 890 g cm^{-2}) as a prototype for constructing an extensive air shower (EAS) array on the Alborz mountain range at an altitude of over 2500 m near Tehran.

The main purpose of this article is to study the unidirectional anisotropy of cosmic ray flow along the Galactic arms, which was observed in the sidereal time at energies above 50 TeV. We describe the experimental setup in Sec. II, and the data analysis and discussion can be found in Sec. III.

II. EXPERIMENTAL SETUP

Four water Cherenkov detectors (WCDs) are used for recording EASs. The four WCDs consist of cylindrical tanks made of polyethylene with a diameter of 64 cm and a height of 130 cm filled up to a height of 120 cm with 382 liters of purified water. All the inner surfaces of the four Cherenkov tanks were optically sealed and covered with white paint which reflects light in a diffusive way. Each one of them has a single 5.2 cm photomultiplier tube (PMT) (model EMI 9813 KB) located at the top of the water level along the cylinder axis. The array was arranged in a square with sides of 608 cm as shown in Fig. 1, on the roof of the Physics Department at Sharif University of

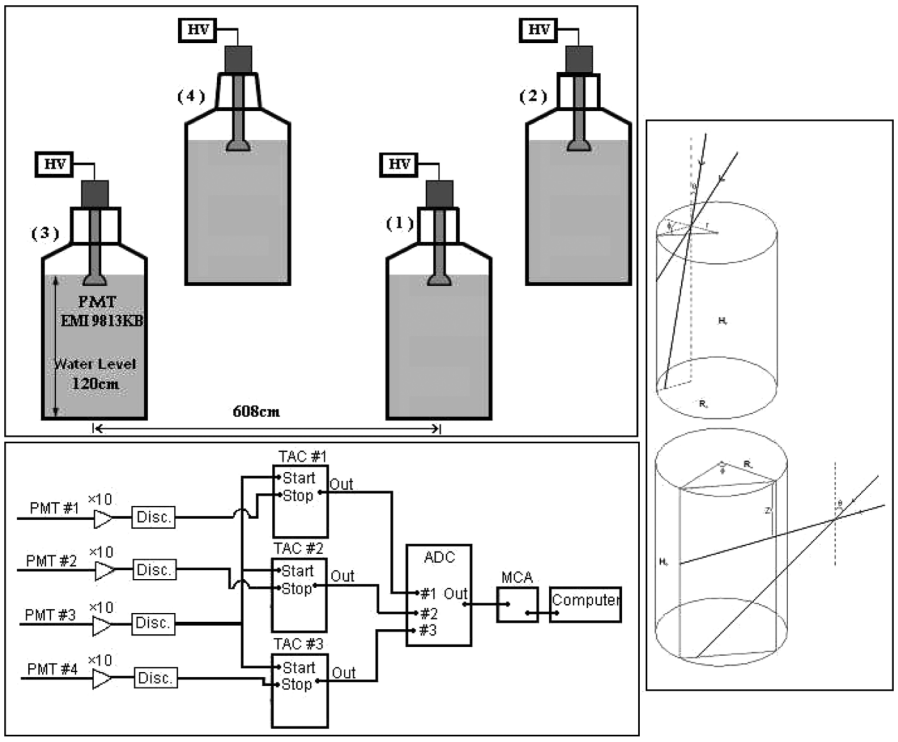

FIG. 1. Schematic view of water Cherenkov detectors as a square array, and the electronic circuit. Particle tracks through the lid (top, right-hand side) and tracks through the walls (bottom, right-hand side) have also been shown.

Technology in Tehran (35°43′ N, 51°20′ E, 1200 m a.s.l = 890 g cm^{-2}). The signal produced by secondary particles of an EAS are triggered with an amplitude threshold of −500 mV by an 8-fold fast discriminator (CAEN N413A). The threshold of each discriminator is set at the separation point between the signal and background noise levels. The discriminator outputs are connected to one of three time to amplitude converters (TAC) (EG&G ORTEC 566) which are set to a full scale of 200 ns (maximum acceptable time difference between two WCDs). The output of the WCD no. 3 is connected to the starting inputs of TAC1, TAC2, and TAC3. The outputs of the WCDs nos. 1, 2, and 4 are, respectively, connected to the stop inputs of TAC1, TAC2, and TAC3. Then the outputs of these three TACs are fed into a multiparameter multichannel analyzer (MCA) (S.R.R. Co.) via an analogue to digital converter (ADC) (S.R.R Co.) unit. The output of TAC1 triggers the ADC, and the three time lags between the output signals of PMTs (3,1), (3,2), and (3,4) are read out as parameters 1 to 3. So by this procedure an event is logged.

III. DATA ANALYSIS AND DISCUSSION

A. Array event rate

The data set covers a total period of 2.7×10^7 seconds. A total of 1.1×10^6 EAS events with arrival direction zenith angles $\leq 60°$ were collected during this time, giving a mean event rate of one event every 24.5 seconds. Figure 2 shows the event time-spacing distribution. Since events arrive randomly in time, it is expected that this will follow an exponential distribution, viz.

$$f(t) = f(0)\exp(-t/\tau). \tag{2}$$

The event rate can be obtained by fitting this function on the event time-spacing distribution. One event per every $\tau = 24.1$ s is obtained from the fit. A nonrandom component for the cosmic ray flux, for example, a point source of a gamma ray, gives rise to deviation from the exponential law. Our observed distribution is in good agreement with the exponential law.

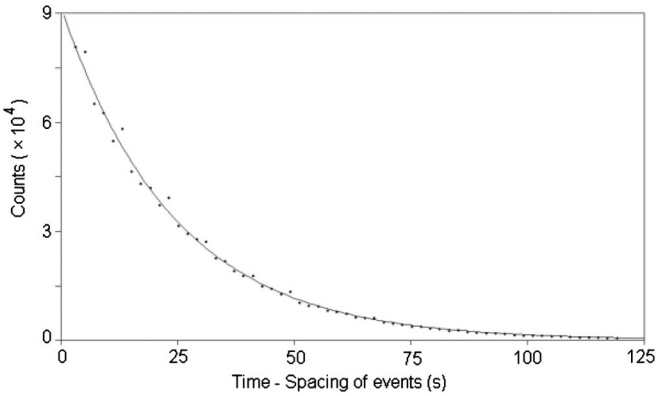

FIG. 2. Distribution of event time-spacing.

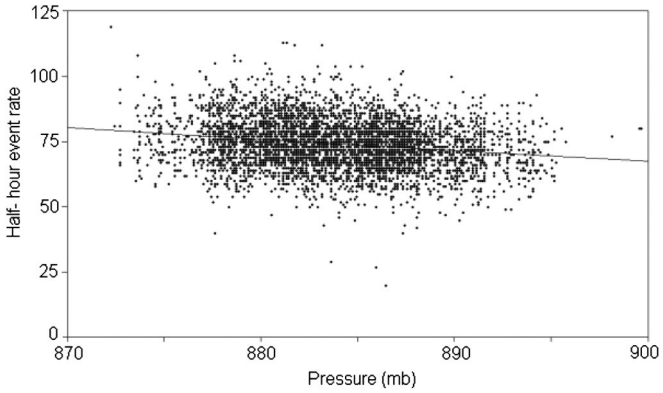

FIG. 3. Event rates per half an hour as a function of atmospheric pressure.

B. Atmospheric effects on the counting rate

The rate of shower detections depends on a number of factors. If either temperature or pressure variations have Fourier components in solar or sidereal times, spurious components may be introduced into the shower detection rate [7]. Various methods are used in order to study the dependence of the event rate on atmospheric ground pressure p and temperature T [15]. In a multiple regression analysis of the event rate against pressure and temperature, the temperature effect is found to be statistically insignificant. The CR intensity dependence on barometric pressures in half-hour intervals is shown in Fig. 3. We can describe the dependence by the following function:

$$R = R_0 \exp\left(\frac{p_0 - p_i}{p_1}\right). \tag{3}$$

The values of $R_0 = 74$ events per half an hour, $p_0 = 883.7$ mb, and $p_1 = 171.5$ mb were obtained from the data. p_i denotes the measured air pressure at a given time. By weighting with this empirical function, we corrected the raw event rates for atmospheric pressure. Figure 4 shows the mean half-hour event rate distributions with and without correction for atmospheric ground pressure. The distribution of corrected rates is consistent with a Gaussian distribution, as expected for the statistical fluctuation of the event rate, and there is no residual temperature effect.

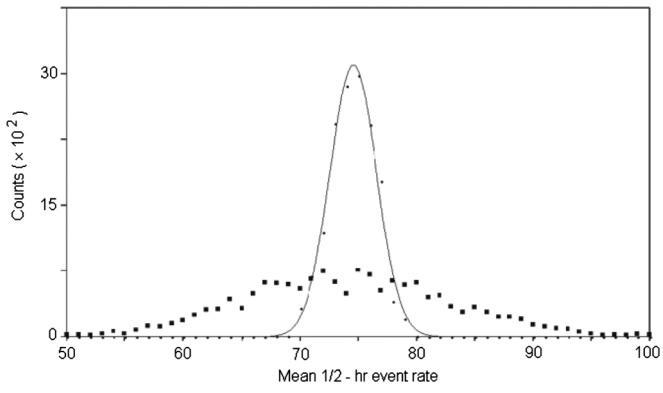

FIG. 4. Distribution of mean 1/2-hour event rates before (squares) and after (points) applying the atmospheric correction for pressure. The solid curve shows a fit by a Gaussian function.

C. Zenith angle distribution of the EAS events

Since the thickness of the atmosphere increases with increasing zenith angle, θ, the number of EAS events is strongly related to θ, as shown in Fig. 5. The differential zenith angle distribution can be represented by

$$dN = \text{constant}(\delta_1 \cos\theta + \delta_2 \sin\theta)\cos^n\theta \sin\theta d\theta, \tag{4}$$

where we split dN into particles entering through the lid of the cylindrical tank of the WCD or through its walls. The first term in parentheses in Eq. (4) is related to the lid and the second to the walls. The parameter δ_1 includes the area of the lid surface, S_1, and detection probability of particles entering through the lid, P_1. The parameter δ_2 also includes the greatest surface area of vertical profile of the WCD, S_2, and detection probability of particles entering through its walls, P_2. So we can write $\delta_j (j = 1, 2)$ in the form

$$\delta_j = S_j P_j, \tag{5}$$

where only P_j's are determined from the simulation (see the Appendix). S_1 and S_2 are, respectively, 3.2×10^3 cm^2 and 7.68×10^3 cm^2. By fitting Eq. (4) on our experimental data, $n = 7.3$ is obtained.

D. Energy threshold of our experiment

Since we cannot determine the energy of the showers on an event-by-event basis, we estimate the energy threshold of our array with the CORSIKA code for simulation of EAS events [16]. In order to record a shower, it is necessary that at least one particle passes through each of the four WCDs. Because our array has been arranged in a square with sides of 608 cm, we can detect a shower if the density of

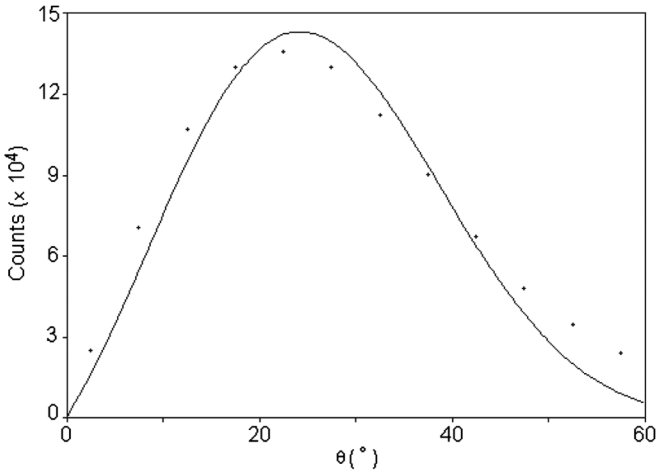

FIG. 5. Frequency of air showers vs zenith angle.

secondary particles is at least $\rho_r = 1/S_{\rm eff}$ particles cm^{-2} at $r = 608 \times \sqrt{2}/2 = 420$ cm, where $S_{\rm eff}$ is the effective surface area of a WCD. This area is calculated as follows:

$$S_{\rm eff} = \frac{\int_0^{\pi/3}(P_1 S_1 \cos\theta + P_2 S_2 \sin\theta)\sin\theta d\theta}{\int_0^{\pi/3}\sin\theta d\theta} = 6.5 \times 10^3 \ {\rm cm}^2, \quad (6)$$

with $P_1 = 0.88$, $S_1 = 3.2 \times 10^3$ cm^2, $P_2 = 0.93$, and $S_2 = 7.68 \times 10^3$ cm^2. The upper limit $\pi/3$ is due to events selection with zenith angles $\leq \pi/3$. We simulated more than 10^5 EAS events with the CORSIKA code using the hadronic interaction models QGSJET and GHEISHA. The energy range for primary particles was selected from 5 TeV to 5 PeV, with differential flux given by $dN/dE \propto E^{-2.7}$. These simulations are in different directions, with a zenith angle from 0° to 60° and an azimuthal angle from 0° to 360°. Finally, from the CORSIKA simulations with $\rho_r = 1.5 \times 10^{-4}$ particles cm^{-2} at $r = 420$ cm, we obtained the energy threshold $E_{\rm th} = 50$ TeV.

E. Sidereal time distribution

After atmospheric correction, we calculated the sidereal time (ST) from ST = ST$_\circ$ + $\alpha(ZT - ZT_0)$. ST$_0$ can be looked up in an almanac [17] for the time ZT_0, ZT is the solar time, and $\alpha = 1.002\,737\,909\,35$. Figure 6 shows percentage variation in intensity of the cosmic rays with sidereal time. *The error bars show the statistical errors only.* The data have been fit to Eq. (7) which describes a curve with first and second harmonics (i.e. with a once-per-day and a twice-per-day variation),

$$y = A_I \cos\left[\frac{2\pi}{24}(t - T_I)\right] + A_{II}\cos\left[\frac{2\pi}{12}(t - T_{II})\right], \quad (7)$$

where t is in hours. The fitting results of data are summarized in Table I. In Fig. 4 we showed a nice narrowing of the rate variation when a pressure correction is applied, by about a factor of 4. But this narrowed distribution still has a FWHM of about $5.1/75 \simeq 7\%$. The width can still have uncorrected contributions to the signal beneath that. As we see from Fig. 6 the coherent anisotropy signal of $\sim$1.7% peak to peak is much less than the width mentioned above. So to have a credible "true sidereal signal" we consider the antisidereal time variation. Because the amplitudes of the antisidereal and spurious sidereal, as a result of the solar seasonal modulation, are equal, the antisidereal acts as a useful indicator of the importance of modulation effects. Our data must therefore be scrutinized for such behavior before ascribing any physical significance to the sidereal vector estimated in the experiment. The antisidereal distribution is also shown in Fig. 7. Sidereal and antisidereal analyses for all showers recorded are shown in Table I. The antisidereal amplitude is small and will not introduce serious irregularities into the sidereal time distribution. We can therefore say we have evidence of a physical anisotropy because the data exhibit a sidereal amplitude $A_I = 0.32 \pm 0.1\%$ and a phase of maximum $= 21.3 \pm 1.0$ hr, when the zenith is toward the Earth's motion. To show the importance of the cosmic ray variation with sidereal time, we split our data sample into two parts. As in Fig. 8 it is observed that the sidereal signal has main features that are

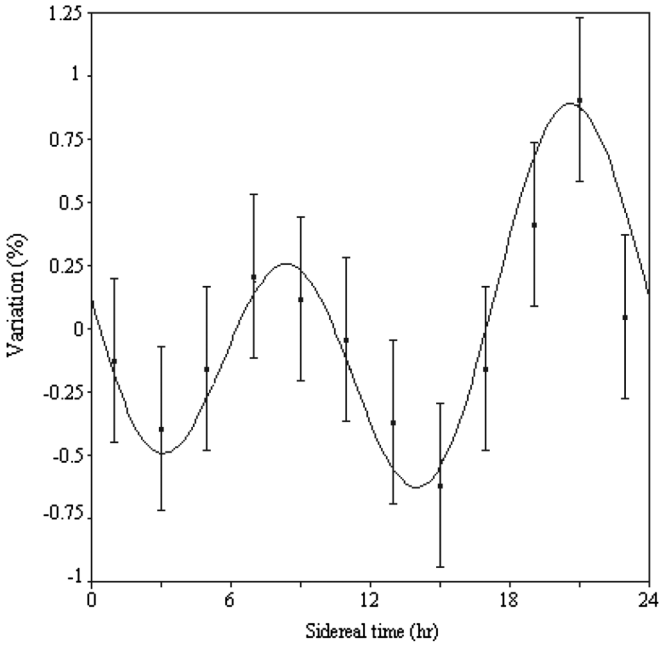

FIG. 6. Observed sidereal time variation in intensity of the cosmic rays (points). The curve is the best fit to Eq. (7) with the coefficients as listed in Table I.

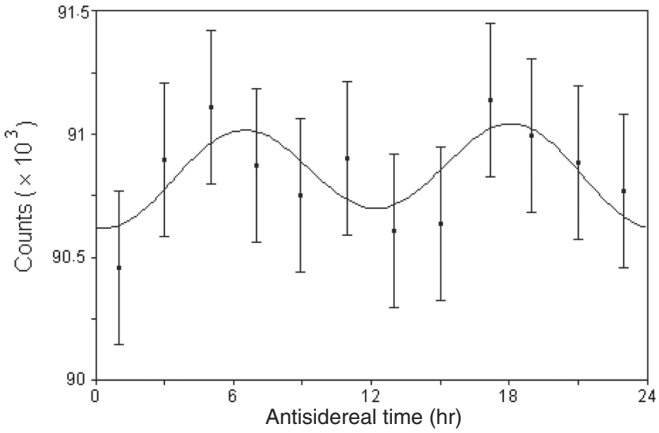

FIG. 7. The antisidereal distribution of cosmic rays detected (points). The curve is the best fit by Fourier expansion up to second harmonic with the coefficients as listed in Table I.

TABLE I. Sidereal and antisidereal analysis of our data.

	First harmonic		Second harmonic	
	Amplitude (%)	Phase (h)	Amplitude (%)	Phase (h)
Sidereal	0.32 ± 0.10	21.3 ± 1.0	0.56 ± 0.10	20.6 ± 0.7
Antisidereal	0.04 ± 0.01	13.5 ± 1.0	0.20 ± 0.05	18.3 ± 1.0

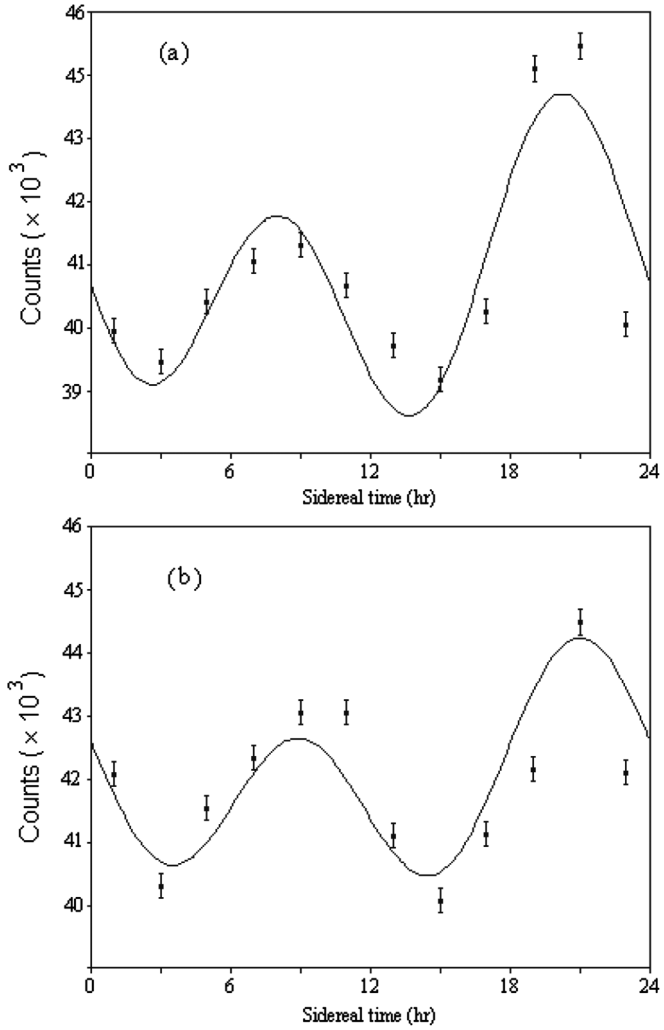

FIG. 8. Observed sidereal time distributions of the cosmic rays (points) to bisect recorded data. The curve is the best fit by Fourier expansion up to second harmonic with the coefficients as listed in Table II.

similar to each other; i.e. the signals are repeated and this means that they are not random. The data analysis is shown in Table II.

The CGE would contribute to the component A_I in the sidereal time asymmetry. As it is seen, there is a definite sidereal time variation whose phase and amplitude are close to those predicted. In order to calculate the magnitude of anisotropy due to CGE, i.e. the value η in Eq. (1), a mean value for $\cos\beta$ is needed. Assume δ is the declination of the direction of the Earth's motion, λ the latitude of the observer, and H the hour angle between the observer's

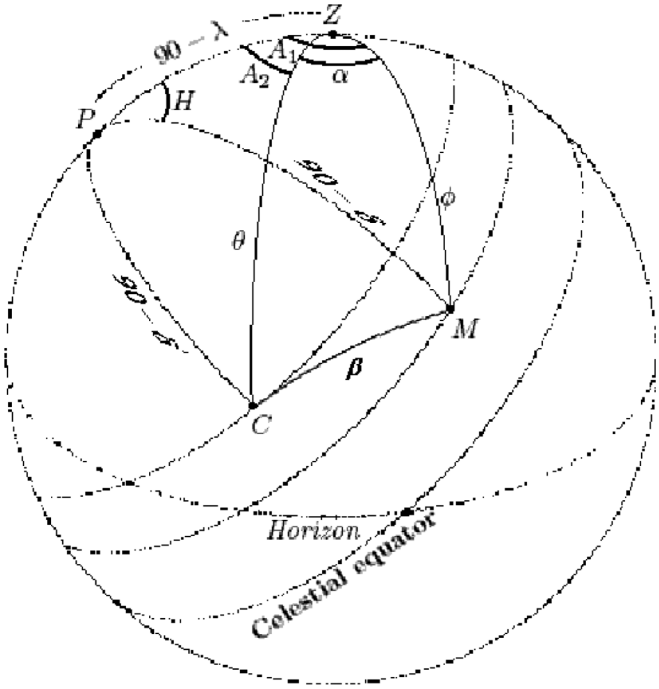

FIG. 9. Celestial coordinate, C = direction of cosmic ray, M = direction of Earth′s motion, Z = zenith, P = direction of North pole.

meridian and the direction of motion; then, considering Fig. 9, the angle ϕ between the observer's zenith and the direction of Earth's motion is given by

$$\cos\phi = \sin\delta\sin\lambda + \cos\delta\cos\lambda\cos H. \tag{8}$$

On the other hand, $\cos\beta$ is calculated by

$$\cos\beta = \cos\phi\cos\theta + \sin\phi\sin\theta\cos\alpha, \tag{9}$$

where θ is the zenith angle of the cosmic ray and α the difference between the azimuthal angle of the direction of motion and that of the cosmic ray (Fig. 9); that is, $\alpha = A_1 - A_2$, where A_1 and A_2 are obtained from

$$\sin\delta = \sin\lambda\cos\phi + \cos\lambda\sin\phi\cos A_1 \tag{10}$$

and

$$\sin\delta' = \sin\lambda\cos\theta + \cos\lambda\sin\theta\cos A_2, \tag{11}$$

where δ' is the declination of the cosmic ray. According to Eqs. (8)–(11), the 24-hour mean of the component of the cosmic ray in the direction of motion ($\cos\beta$) may be obtained. Using $\lambda = 35°43'$ and $\delta = 47°$, we calculated the 24-hour mean value of $\cos\phi \simeq 0.43$ with Eq. (8). With

TABLE II. The sidereal analysis of two parts of our data.

Sidereal	First harmonic Amplitude (%)	Phase (h)	Second harmonic Amplitude (%)	Phase (h)
First part (a)	0.27 ± 0.40	21.1 ± 1.0	0.52 ± 0.30	20.2 ± 1.0
Second part (b)	0.28 ± 0.40	21.4 ± 1.0	0.50 ± 0.30	21.0 ± 1.0

the distribution of $(P_1S_1\cos\theta + P_2S_2\sin\theta)\cos^{7.3}\theta\sin\theta$ which describes the acceptance of detectors and the cosmic ray absorption in the Earth's atmosphere because of inclination from the vertical direction in Tehran (Sec. III C), we calculated the mean value of $\cos\theta = 0.88$. Also, the mean values of A_1 and A_2 were obtained by using the mean value δ'. Figure 10 shows the distribution of cosmic ray declination. The mean value of declination is $\delta' = 32.5°$. From Eqs. (10) and (11), A_1 and A_2 were obtained to be 49° and 86°, respectively. Finally, from Eq. (9) a value of 0.72 was obtained for $\cos\beta$, and this was multiplied by the expected CGE amplitude of 0.345% to yield a predicted effect of expected value of 0.248%. The value obtained from experimental data is 0.32% which is about 0.07% more than the CGE value. This remaining asymmetry of 0.07% presumably has an origin different than that of the CGE.

Since the cosmic ray data have been recorded in Tehran with the latitude 35°43′ N, the majority of cosmic rays are from the spiral arm inward direction, which is at about 20 hours in right ascension and 35° in declination [18]. So the remaining asymmetry is probably due to unidirectional anisotropy of cosmic ray flow along the Galactic arms. A simple diffusion model [19] suggests that the value of this asymmetry, 0.07%, would be roughly equal to the ratio of the scattering mean free path to a characteristic dimension of the containment region (i.e. the central Galactic region, with a scale of 10 kpc). So, with the amplitude of the anisotropy of 0.07% found in this work, we obtain a mean free path of about 7 pc which is about perhaps 7 times of gyro radius.

Since the anisotropies are low, it is necessary to consider the effect of counting statistics for a finite measured data set. If we have N events, then the probability of getting a fractional amplitude greater than r is given by [20]

$$P(>r) = e^{-k_0}, \qquad k_0 = r^2N/4. \tag{12}$$

So, a convenient parameter for characterizing the anisotropy amplitude probability distribution is k_0. We can take $\sqrt{2}r_{\rm rms}$, which corresponds to $k_0 = 1$, as the noise amplitude. For the number of events that we have accumulated, 1.1×10^6, the total amplitude of 0.32% obtained in this work can arise by chance with a probability of ~0.06 corresponding to $k_0 = 2.8$. This shows a significant anisotropy ($k_0 > 1$) during the sidereal period. So we conclude that this data set gives evidence of anisotropy.

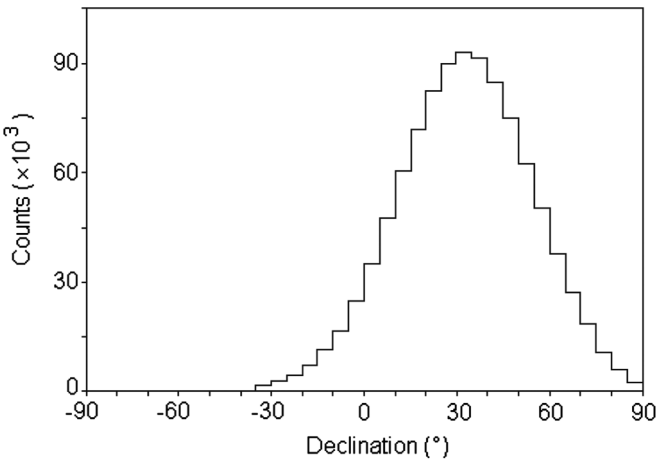

FIG. 10. Distribution of air shower events vs declination angle.

IV. CONCLUSION

Cosmic ray data in the Alborz observatory clearly show an anisotropy in sidereal time with an energy threshold of ~50 TeV and a mean energy of ~121 TeV. One part of this anisotropy is due to the Earth's motion around the Galaxy (the CGE), but our measured asymmetry suggests the possible existence of some other additional effects, probably a unidirectional anisotropy of cosmic ray flow along the Galactic arms. The first harmonic amplitude of our total measured anisotropy is about 0.32%. The CGE contribution to this anisotropy is about 0.248%, and the rest, 0.07%, is predicted to be due to the flow along the Galactic arm. The latter anisotropy suggests a mean free path of about 7 pc for these high-energy cosmic rays. The evidence of these anisotropies is based on the value of the parameter k_0, as suggested by Linsley (1975), and found in this work to be 2.8, that is, more than $k_0 = 1$, the value for the noise amplitude.

The EAS-TOP experiment reported somewhat lower limits in the energy range below 1200 TeV [21]. The relatively large amplitudes published by the Akeno experiment [13] and our experiment are difficult to reconcile with the results of the EAS-TOP experiment.

ACKNOWLEDGMENTS

This research has been partly supported by Grant No. NRCI 1853 of the National Research Council of Islamic Republic of Iran.

APPENDIX

In order to obtain the P_j's, Eq. (5), we first calculated the track length in water of a particle passing through the lid and walls of a WCD. To determine the track length distribution we have made the following assumptions:

(A) The zenith and azimuthal angles of particles are uniformly distributed.

(B) The random distribution increases linearly with r, the distance from the center of the lid; i.e. it is proportional to the annulus surface $2\pi r\Delta r$.

The geometry can be simply solved. It is split into particles entering through the lid or through the walls as seen in Fig. 1. In these figures, r is the distance from the center of the cylinder, the tank radius is $R_0 = 32$ cm, the tank height $H_0 = 120$ cm, and φ and θ are azimuthal and zenith angles of the particle, respectively. The simulation process starts by randomly choosing r which increases linearly with r. Then φ and θ are randomly chosen and

the track lengths within the tank are evaluated by a simple calculation (the particle could either leave through the wall or the bottom lid, as shown in Fig. 1).

Then the number of photons produced along a flight path is estimated. Charged particles emit light under a characteristic angle when passing through a medium if their velocity exceeds the speed of light in the medium. The Cherenkov angle is related to the particle velocity and the refractive index of the medium $n(\cos\theta = 1/n\beta)$. For relativistic particles, $\beta = 1$, and the refractive index of purified water, $n = 1.33$ (for short wavelengths of visible region), the Cherenkov light is emitted under 41°. The number of photons produced along a flight path dx in a wavelength bin $d\lambda$ for a particle carrying unit charge is

$$\frac{d^2N}{dxd\lambda} = \frac{2\pi\alpha\sin^2\theta}{\lambda^2}, \tag{13}$$

where $\alpha = 1/137$. At wavelengths of 310–470 nm the efficiency of the photomultiplier is maximal. Within a 1 cm flight path 220 photons are emitted in this wavelength bin. Considering the effective area of the photomultiplier (21.2 cm^2) and neglecting absorption and scattering effects in water, we obtained the number of photons received by PMT (Fig. 9). Finally, with a $\eta = 25\%$ quantum efficiency and a $G = 10^8$ gain for the PMT, the number of electrons produced in PMT ($N_e = N_{\text{photon}}\eta G$) was calculated. As we know, the output signal at the PMT's anode is a current or charge pulse. Now, considering the amplitude threshold of the discriminator ($-$ 500 mV) and the anode load resistor and capacitance, we obtain that, for producing a pulse with amplitude -500 mV, the number of photons received by PMT should be more than 1. Since the quantum efficiency of the PMT is 25%, using Fig. 11 we calculated the detection probabilities P_j's as, respectively, 0.88 and 0.93 for the lid and the walls of the WCD.

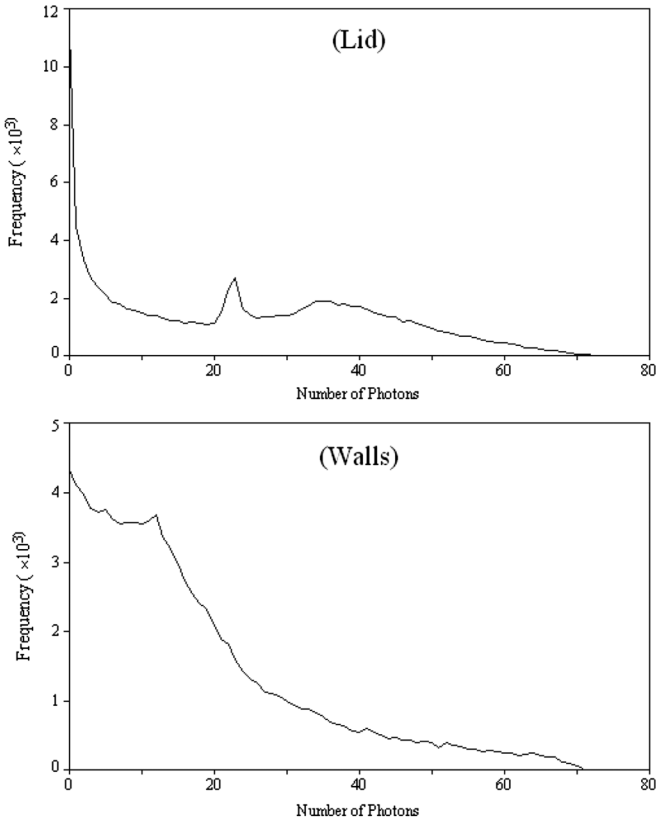

FIG. 11. The number of photons received by PMT as a consequence of particles passing along different tracks entering through the lid (top panel) and the walls (bottom panel) of the WCD.

[1] J. W. Armstrong, B. J. Rickett, and S. R. Spangler, Astrophys. J. **443**, 209 (1995).
[2] V. S. Ptuskin, Adv. Space Res. **19**, 697 (1997).
[3] A. G. K. Smith and R. W. Clay, Aust. J. Phys. **50**, 827 (1997).
[4] A. H. Compton and I. A. Getting, Phys. Rev. **47**, 817 (1935).
[5] J. Poirier and C. D'Andrea, and M. Dunford, Proceedings of the 27th ICRC, Hamburg, Germany, 2001, p. 3930.
[6] T. F. Lin *et al.*, Proceedings of the 26th ICRC, Salt Lake City, 1999, Vol. 2, p. 100.
[7] F. J. M. Farley and J. R. Storey, Proc. Phys. Soc. London Sect. A **67**, No. 11, 996 (1954).
[8] H. Kojima *et al.*, Proceedings of the 27th ICRC, Hamburg, Germany, 2001, Vol. 10, p. 3943.
[9] H. Kojima *et al.*, Proceedings of the 28th ICRC, Tsukuba, Japan, 2003, Vol. 7, p. 3957.
[10] K. Nagashima *et al.*, Nuovo Cimento Soc. Ital. Fis. **12C**, 695 (1989).
[11] K. Nagashima, K. Fujimoto, and R. M. Jacklyn *et al.*, J. Geophys. Res. **103**, 17429 (1998).
[12] M. Aglietta *et al.*, Astrophys. J. **470**, 501 (1996).
[13] T. Kifune *et al.*, J. Phys. G **12**, No. 2, 129 (1986).
[14] R. Clay *et al.*, Proceedings of the 25th ICRC, Durban, 1997, Vol. 4, p. 185.
[15] T. Antoni *et al.*, Astrophys. J. **604**, 687 (2004).
[16] D. Heck *et al.*, Report No. FZKA6019 (Forschungszentrum Karlsruhe), 1998.
[17] tycho.usno.navy.mil/sidereal.html.
[18] R. M. Jacklyn, PASA **6**, 425 (1986).
[19] H. R. Allan, Astrophys. Lett. **12**, 237 (1972).
[20] J. Linsley, Phys. Rev. Lett. **34**, 1530 (1975).
[21] M. Aglietta *et al.* (EAS-TOP Collaboration), Proceedings of the 28th ICRC, Tsukuba, Japan, 2003, Vol. 4, p. 183.